Proceedings of the
International Conference on Mechanical Engineering 2003
(ICME2003) 26- 28 December 2003, Dhaka, Bangladesh

ICME03-FL-15

EFFECT OF NON-EQUILIBRIUM CONDNESATION ON COMPRESSIBLE FLOWS IN AN EXPANSION TUBE WITH AN ORIFICE

Shigeru MATSUO[1], Masanori TANAKA[1], Mamun MOHAMMAD[1], Toshiaki SETOGUCHI[1] and Heuy-Dong KIM[2]

[1]Dept. of Mechanical Engineering, Saga University, 1 Honjo-machi, Saga-shi, Saga 840-8502, Japan,
[2]School of Mechanical Engineering, Andong National University, 388, Songchun-dong, Andong, 760-749, Korea.

ABSTRACT

In the present study, a computational fluid dynamics work was applied to clarify the effect of non-equilibrium condensation on compressible flows in an expansion tube with an orifice. A third-order TVD finite difference scheme with MUSCL was used to discretize the spatial derivatives, and a second order-central difference scheme for the viscous terms. A second-order fractional step was employed for time integration. To close the governing equations above, Baldwin-Lomax model was employed in computations. As a result, it is clarified that the compressible flow around the orifice is strongly influenced by the non-equilibrium condensation.

Keywords: Compressible flow, Orifice, Non-equilibrium Condensation.

1. INTRODUCTION

Many studies on the propagation of the unsteady expansion wave in a pipe with area changes have been performed [1-5] until now. However, there are few studies on the interaction of the unsteady expansion wave with orifices in a pipe, which occurs in the piping system of reciprocating engines, railway's pneumatic air brake system, rapid opening of valve and a burst of high pressure tubes [6-10]. This study is important not only for mechanical application, but also for basic research in gasdynamics.

A rapid expansion of moist air or steam in a supersonic nozzle and shock tube gives rise to non-equilibrium condensation [11-13]. In the shock tube, it is known that the non-equilibrium condensation occurs in an unsteady accelerated flow induced by an expansion fan in a driver section [14-17]. However, there are many questions that are not yet resolved about the effects of the non-equilibrium condensation on the unsteady accelerated flow with the orifice in a pipe.

In the present study, a computational fluid dynamics work was applied to clarify the effect of non-equilibrium condensation on compressible flows in an expansion tube with an orifice, and the time - dependent static pressure, Mach number and non-equilibrium condensation properties like the condensate mass fraction, were discussed based upon the present computational results.

2. CFD ANALYSIS

2.1 Governing Equations

Assumptions using in the present calculation of the two phase flow are as follows ; Both velocity slip and temperature difference do not exist between condensate particles and gas mixture, and the effect of the condensate particles on pressure is neglected. The governing equations are the unsteady compressible Navier - Stokes equations and droplet growth equation [14] written in an axisymmetric coordinate system (x,y) (y : radial distance from the center line) as follows;

$$\frac{\partial \boldsymbol{U}}{\partial t}+\frac{\partial \boldsymbol{E}}{\partial x}+\frac{\partial \boldsymbol{F}}{\partial y}=\frac{1}{Re}\left(\frac{\partial \boldsymbol{R}}{\partial x}+\frac{\partial \boldsymbol{S}}{\partial y}\right)+\frac{1}{y}H+Q \tag{1}$$

where

$$\boldsymbol{U}=\begin{bmatrix}\rho_m\\ \rho_m u\\ \rho_m v\\ E_s\\ \rho_m g\\ \rho_m D_1\\ \rho_m D_2\\ \rho_m D_3\end{bmatrix},\ \boldsymbol{E}=\begin{bmatrix}\rho_m u\\ \rho_m u^2+p\\ \rho_m uv\\ u(E_s+p)\\ \rho_m ug\\ \rho_m uD_1\\ \rho_m uD_2\\ \rho_m uD_3\end{bmatrix},\ \boldsymbol{F}=\begin{bmatrix}\rho_m v\\ \rho_m uv\\ \rho_m v^2+p\\ v(E_s+p)\\ \rho_m vg\\ \rho_m vD_1\\ \rho_m vD_2\\ \rho_m vD_3\end{bmatrix} \tag{2}$$

$$\boldsymbol{R}=\begin{bmatrix}0\\ \tau_{xx}\\ \tau_{xy}\\ \alpha\\ 0\\ 0\\ 0\\ 0\end{bmatrix},\boldsymbol{S}=\begin{bmatrix}0\\ \tau_{yx}\\ \tau_{yy}\\ \beta\\ 0\\ 0\\ 0\\ 0\end{bmatrix},\boldsymbol{H}=\begin{bmatrix}-\rho v\\ -\rho uv\\ -\rho v^2\\ -v(E_t+p)\\ 0\\ 0\\ 0\\ 0\end{bmatrix},\boldsymbol{Q}=\begin{bmatrix}0\\ 0\\ 0\\ 0\\ \rho_m\dot{g}\\ \rho_m\dot{D}_1\\ \rho_m\dot{D}_2\\ \rho_m\dot{D}_3\end{bmatrix} \tag{3}$$

where

$$E_s = \rho_m C_{p0} T + \frac{1}{2}\rho_m \left(u^2 + v^2\right) - \rho_m g L \tag{4}$$

$$p = G\left[E_t - \frac{1}{2}\rho_m \left(u^2 + v^2\right) + \rho_m g L\right] \tag{5}$$

$$G = \left(1 - g\frac{M_m}{M_v}\right) \Big/ \left(\frac{1}{\gamma - 1} + g\frac{M_m}{M_v}\right) \tag{6}$$

$$\alpha = u\tau_{xx} + v\tau_{yx} + k\frac{\partial T}{\partial x}, \quad \beta = u\tau_{xy} + v\tau_{yy} + k\frac{\partial T}{\partial y} \tag{7}$$

where τ_{xx}, τ_{xy}, τ_{yx} and τ_{yy} are components of viscous shear stress. Subscripts m and v refer to mixture and vapor, respectively. k is thermal conductivity. The latent heat L is given by a function of temperature [19] ;

$$L(T) = L_0 + L_1 T \quad \text{J/kg} \tag{8}$$

$$L_0 = 3105913.39 \ \text{J/kg}, \quad L_1 = -2212.97 \ \text{J/kg}$$

The condensate mass fraction g is given by a rate equation, expressed by Eq.(9) [14].

$$\dot{g} = \frac{dg}{dt} = \frac{\rho_l}{\rho_m}\left(\frac{4\pi}{3} r_c^{\ 3} I + \rho_m D_1 \frac{dr}{dt}\right) \tag{9}$$

In Eq.(3), $\dot{D}_1$, $\dot{D}_2$, and $\dot{D}_3$ are given as:

$$\dot{D}_1 = \frac{dD_1}{dt} = \frac{4\pi\, r_c^{\ 2} I}{\rho_m} + D_2 \frac{dr}{dt} \tag{10}$$

$$\dot{D}_2 = \frac{dD_2}{dt} = \frac{8\pi\, r_c I}{\rho_m} + D_3 \frac{dr}{dt} \tag{11}$$

$$\dot{D}_3 = \frac{dD_3}{dt} = \frac{8\pi\, I}{\rho_m} \tag{12}$$

Nucleation rate I, critical radius of the nuclei r_c and radius growth rate $\dot{r}$ are given as [14][19] follows :

$$I = \frac{1}{\rho_l}\left(\frac{2 m_v \sigma}{\pi}\right)^{1/2}\left(\frac{p_v}{\kappa T}\right) exp\left(\frac{-4\pi\, r_c \sigma}{3T\kappa}\right) \tag{13}$$

$$r_c = \frac{2\sigma}{\rho_l \Re_v T\, ln\left(p_v / p_{s,\infty}\right)} \tag{14}$$

$$\dot{r} = \frac{dr}{dt} = \frac{1}{\rho_l}\frac{p_v - p_{s,r}}{\left(2\pi \Re_v T\right)^{1/2}} \tag{15}$$

In the above equations, m, κ, $\Re$ and $p_{s,\infty}$ are the molecular weight, Boltzmann constant, the gas constant and the flat film equilibrium vapor pressure, respectively. The density of liquid phase is given by a function of temperature [19] ;

$$\left.\begin{aligned} \rho_l(T) &= \frac{A_0 + A_1 t + A_2 t^2 + A_3 t^3 + A_4 t^4 + A_5 t^5}{1 + B_0 t} \quad \text{kg/m}^3,\ (t \geq 0\ ^\circ\text{C}) \\ \rho_l(T) &= A_6 + A_7 t + A_8 t^2 \quad \text{kg/m}^3,\ (t < 0\ ^\circ\text{C}) \end{aligned}\right\} \tag{16}$$

where t is the temperature given by °C and the coefficients are given by :

$A_0 = 999.8396$, $A_1 = 18.224944$,
$A_2 = -7.92221 \times 10^{-3}$, $A_3 = -55.44846 \times 10^{-6}$,
$A_4 = 149.7562 \times 10^{-9}$, $A_5 = -393.2952 \times 10^{-12}$,
$A_6 = 999.84$, $A_7 = 0.086$, $A_8 = -0.0108$,
$B_0 = 18.159725 \times 10^{-3}$

The surface tension σ $(= \sigma_\infty)$, that is an infinite flat-film surface, is given by ;

$$\left.\begin{aligned} \sigma_\infty(T) &= \{76.1 + 0.155(273.15 - T)\} \times 10^{-3}, \quad \text{for } T \geq 249.39 \ \text{K} \\ \sigma_\infty(T) &= \{(1.1313 - 3.7091 \times 10^{-3} \times T) \times T^4 \times 10^{-4} - 5.6464\} \times 10^{-6}, \quad \text{for } T < 249.39 \ \text{K} \end{aligned}\right\} \tag{17}$$

In Eq.(14), $p_{s,\infty}$ is also given as [19] :

$$p_{s,\infty}(T) = exp\left(A_9 + A_{10} T + A_{11} T^2 + B_1 ln(T) + \frac{C_0}{T}\right) \quad \text{N/m}^3 \tag{18}$$

$A_9 = 21.125$, $A_{10} = -2.7246 \times 10^{-2}$,
$A_{11} = 1.6853 \times 10^{-5}$, $B_1 = 2.4576$, $C_0 = -6094.4642$

where T is given by the temperature (K). Using flat film equilibrium vapor pressure $p_{s,\infty}$ above, the saturation vapor pressure $p_{s,r}$ of condensate droplet with a radius of r in Eq.(15) is given by Thompson-Gibbs equation [14] ;

$$p_{s,r} = p_{s,\infty}\, exp\left(\frac{2\sigma_\infty}{\rho_l \Re_v T r}\right) \tag{19}$$

The governing equation systems that are non-dimensionalized with reference values at the inlet conditions upstream of the nozzle are mapped from the physical plane into a computational plane of a general transform. To close the governing equations, Baldwin-Lomax model [20] is employed in computations. A third-order TVD (Total Variation Diminishing) finite difference scheme with MUSCL [21] is used to discretize the spatial derivatives, and a second order-central difference scheme for the viscous terms, and a second-order fractional step is employed for time integration.

The validity of the method used in the present calculation is shown in the previous research [18].

2.2 Computational Conditions

Figure 1 shows computational grids of an expansion tube with an orifice. The number of grids is 640×121. The shock tube has a diameter of $\phi\, D$=65.8 mm and a length of L=5251 mm. A diaphragm located at an origin (x=0 mm) in the present computation, separates the high

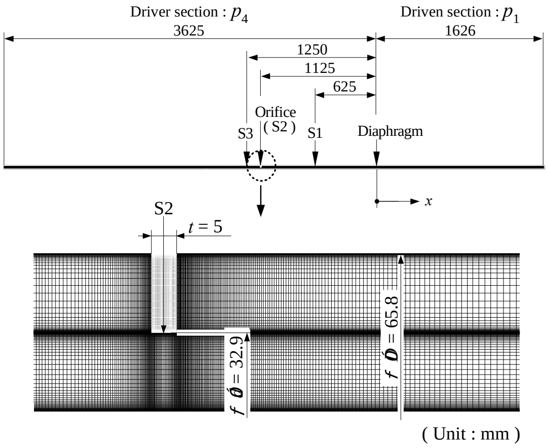

Fig.1 Computational grid

(driver section : 3625 mm) and low pressure (driven section : 1626 mm) sides. The pressures in the high and low pressure tubes are denoted as p_4 and p_1, respectively. The orifice is located at x = -1125 mm. The orifice diameter and thickness are 32.9 mm and 5 mm, respectively.

In the present study, moist air is used as a working gas and assumed to be thermally and calorically perfect. p_4 is kept constant at 101.3 kPa and values of p_4/p_1 (p_{41}) are 3 and 5. Temperature T_4 in the high pressure side is 298 K. Values of the initial degree of supersaturation S_0 ($= p_{v0} / p_{s,\infty}$) are 0 and 0.7. Inlet boundary is constrained with wall boundary condition and exit boundary is constrained with free boundary condition. Non-slip velocity and no heat transfer are constrained on the solid wall. Condensate mass fraction g=0 is set at the wall.

3. RESULTS AND DISCUSSION

At the each location along the centerline of the expansion tube, variations of the computed static pressure p with time for p_{41} = 3 and 5 are shown in Figs.2 and 3 (see the positions S1, S2 and S3 denoted in Fig.1), respectively. Here t indicates the time elapsed from the moment of rupture of the diaphragm. The broken and solid lines are the static pressure for S_0=0 (dry air) and 0.7, respectively. In the lower part in each figure, static pressure distribution at the position S3 is shown after magnification.

In both figures, static pressures at the position S1 for S_0=0 decrease monotonously due to unsteady expansion wave and then change largely due to the influence of orifice flow. For S_0=0.7, static pressures increase due to the non-equilibrium condensation in expansion wave [17] and then change largely in the same manner as that for S_0=0. At the position S3 in Fig.2 (p_{41}=3), the static pressures for S_0=0 and 0.7 fluctuate even upstream of the orifice. However, the fluctuation of the static pressures in Fig.3 (p_{41}=5) is smaller than that in Fig.2 (p_{41}=3).

Figures 4 and 5 show wave diagrams for the static pressures p along the center-line of the expansion tube in the range of t = 0.009 s – 0.011 s for p_{41} = 3 and 5, respectively. Here x indicates a distance from the position of the diaphragm along the tube. Figs.4(a) and 5(a) show the case of S_0=0 (without the non-equilibrium condensation), and Figs.4(b) and 5(b) for the case of S_0=0.7 (with the non-equilibrium condensation).

In Figs.4(a) and (b), variations of static pressures are not seen clearly upstream of orifice. However, there are small variations in the static pressure as described in Fig.2. From Fig.4(b), it is found that the static pressure oscillates just downstream of the orifice periodically. The oscillation is responsible for the periodic excursions of the compression wave by the non-equilibrium condensation. The frequency of oscillation is about 5 KHz. From FFT analysis (t = 0.009 s – 0.011 s) of pressure signals at the position S3 in Fig.2(a), a peak of spectrum was obtained at the same frequency to it. This means that the oscillation by the non-equilibrium condensation including the oscillation of shear layer propagates upstream of the orifice. This is because that the flow is not choked at the orifice position as will be described later. In Fig.5(b), the oscillation of static pressure by the non-equilibrium condensation is not observed behind the orifice in comparison with Fig.4(b).

Furthermore, it was found in the range of x/D > -16.7

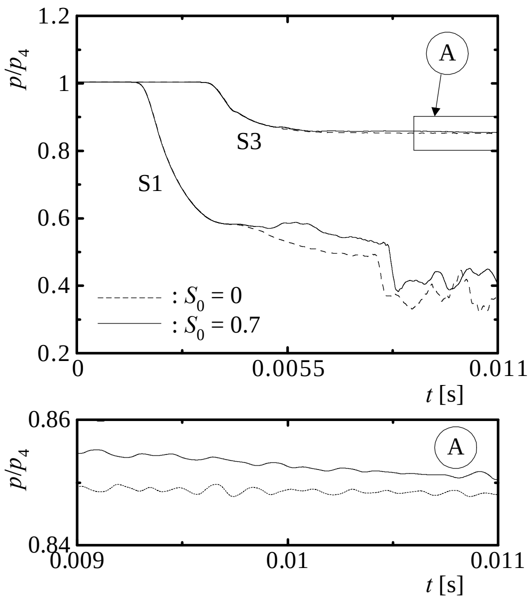

Fig.2 Time histories of static pressure (p_{41} = 3)

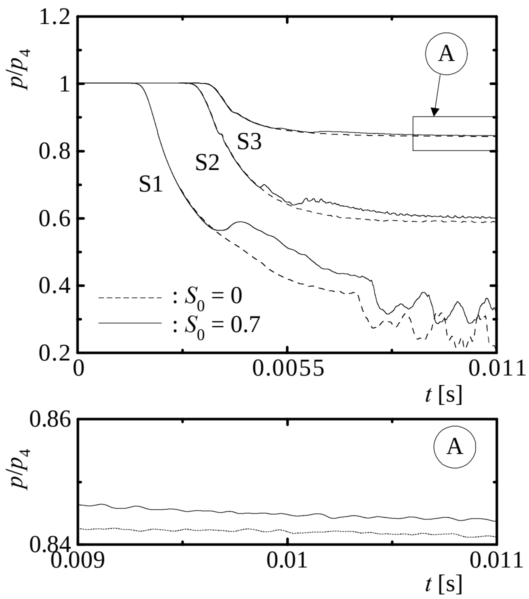

Fig.3 Time histories of static pressure (p_{41} = 5)

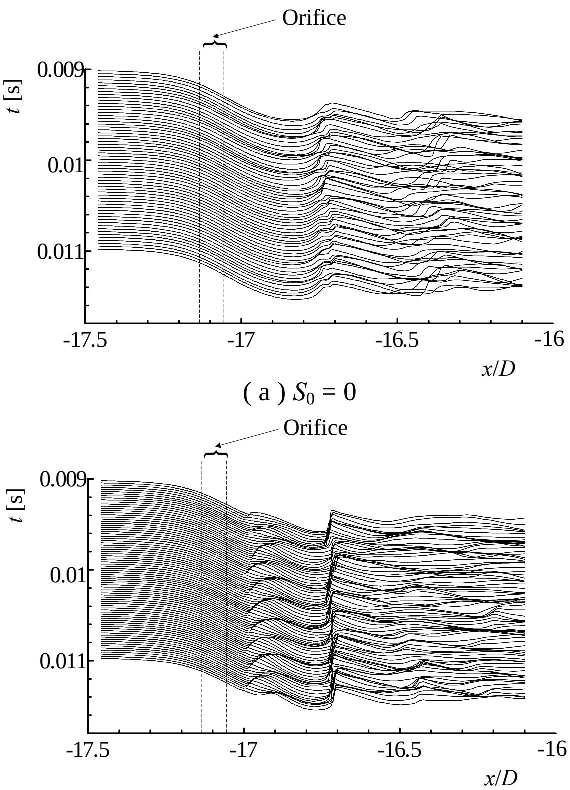

(a) S_0 = 0

(b) S_0 = 0.7

Fig.4 Static pressure wave diagram (p_{41} = 3)

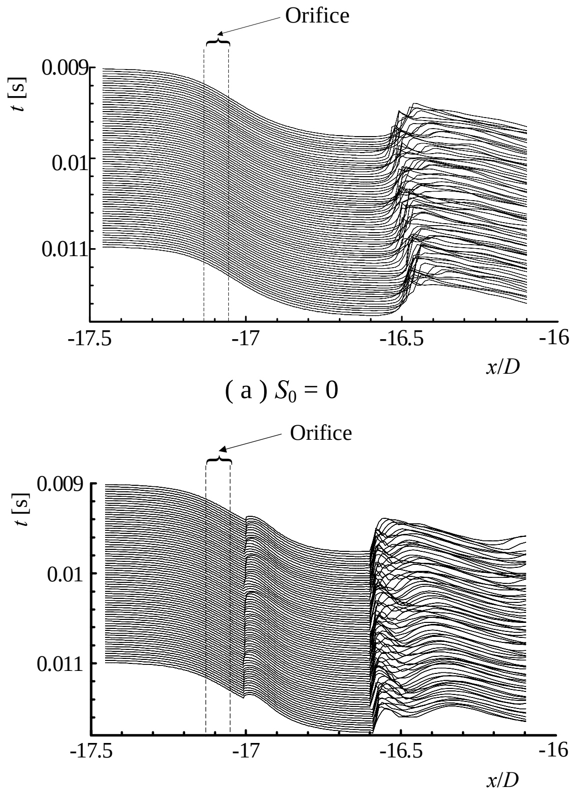

(a) S_0 = 0

(b) S_0 = 0.7

Fig.5 Static pressure wave diagram (p_{41} = 5)

for p_{41} = 3 that pressure variations Δp in case of S_0=0.7 (non-equilibrium condensation) became small in comparison with the case of S_0=0.

Figure 6(a) shows distributions of Mach number for one cycle of the oscillation corresponding to Fig.4(b). In Fig.6(b), contour maps of the condensate mass fraction for one cycle are shown and broken lines denote the sonic line. From Fig.6(a), it is found that the flow is not choked at the position of orifice and Mach number downstream of the orifice for S_0 = 0.7 changes largely in comparison with the case of S_0=0. In Fig.6(b), the condensate mass fraction begins to increase at the location close to the leading edge of the orifice. The sonic line changes largely and does not reach the orifice surface.

Figure 7(a) shows distributions of Mach number corresponding to Fig.5(b). Contour maps of condensate mass fraction are shown in Fig.7(b). From the reason that the degree of flow expansion behind the orifice becomes large in comparison with Fig.6 (p_{41} = 3), the sonic line close to the orifice hardly change in comparison with the case of Fig.6(b), and approaches the orifice surface in comparison with Fig.6(b).

4. CONCLUSIONS

In the present study, a computational fluid dynamics work was applied to clarify the effect of non-equilibrium condensation of moist air on compressible flows in an expansion tube with an orifice. The results obtained are summarized as follows ; for low pressure ratio with the non-equilibrium condensation, periodic excursions of the compression wave by the non-equilibrium condensation occur just downstream of the orifice and the sonic line downstream of the orifice changes largely in comparison with the case of dry air. The periodic oscillation propagates upstream through the orifice. For high pressure ratio, there are no periodic oscillations by the non-equilibrium condensation and the flow around the orifice is stable.

5. REFERENCES

1. Glass, I. I. and Patterson, G. N., 1955, "A Theoretical and Experimental Study of Shock-Tube Flows", Journal of the Aeronautical Sciences, 22-2:73-100.
2. Billington, I. J., 1956, "An Experimental Study of the One-Dimensional Refraction of a Rarefaction Wave at a Contact Surface", 1956, 997-1006.
3. Levy, M. J. and Potter, J. H., 1964, "Some Transient Measurements in a Rarefaction Wave Tube", Journal of Engineering for Industry, 365-370.
4. Levy, M. J. and Potter, J. H., 1964, "Gas Flow in a Rarefaction Wave Tube", Naval Engineers Journal, 941-950.
5. Hall, J. G., Srinivasan, G. and Rathi, J. S., 1974, "Unsteady Expansion Waveforms Generated by Diaphragm Rupture, AIAA Journal, 12-5:724-726.
6. Male, D. H., Chelsom, R. A. and Deckker, B. E. L., 1969-1970, "Behaviour of Rarefaction Waes at the Junction of a Branched Duct", Proc. Instn. Mech. Engrs, 184-Pt3G:1-6.
7. Kage, K., Kawagoe, S., Matsuo, K. and Hasegawa, I., 1989, "A Theoretical Study of Moving Expansion Waves in a Branched Duct", *Proc. First JHPS International Symposium on Fluid Power Tokyo,*

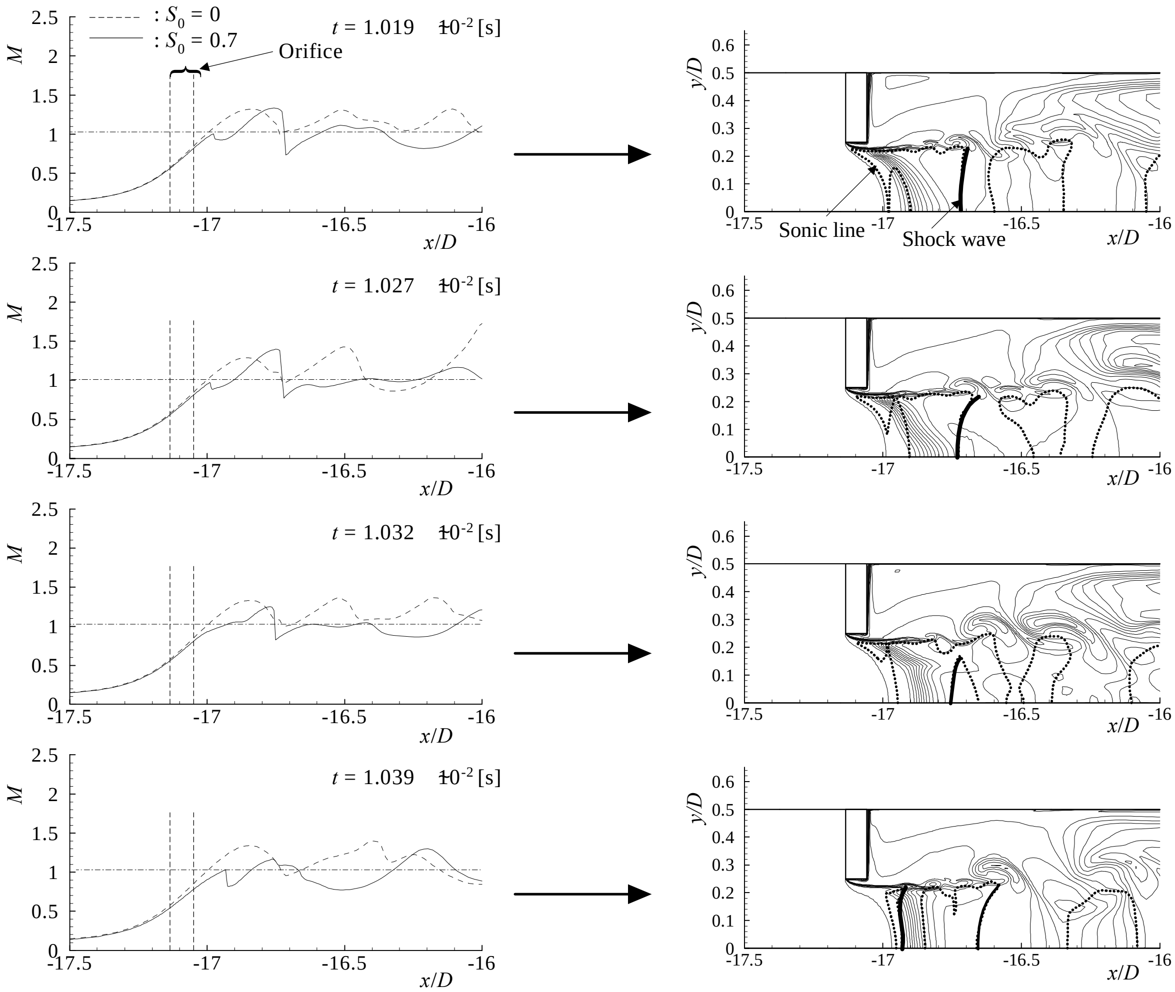

(a) Distribution of Mach number

(b) Contour maps of condensate mass fraction

Fig.6 Time variation of Mach number and condensate mass fraction (p_{41} = 3 , S_0 = 0.7)

287-292-137.

8. Tanaka, H., Hasegawa, I., Kage, K., Kawagoe, S. and Matsuo, K., 1986, "A Study on Characteristics of Pressure Reduction of Compressed Air in a Long Pipe", 52-474:772-776.
9. \\\aka, H., Hasegawa, I., Kage, K., Kawagoe, S. and Matsuo, K., 1986, "A Study on Characteristics of Pressure Reduction of Compressed Air in a Long Pipe", 52-481:3181-3185.
10. Flatt, R., 1986, "Unsteady Compressible Flow in Long Pipelines Following a Rupture", International Journal for Numerical Mehods in Fluids, 6:83-100.
11. Wegener, P. P. and Mack, L.M., 1958, *Condensation in supersonic hypersonic wind tunnels*, Adv. In Applied Mechanics, 5, Academic Press, New York.
12. Matsuo, K., Kawagoe, S., Sonoda, S. and Sakao, K., 1985, "Studies of Condensation Shock Waves (Part1, Mechanism of their Formation)", Bulletin of JSME 28:2577-2582.
13. Schnerr, G. H., 1986, "Homogene Kondensation in Stationären Transsonischen Strömungen durch Lavaldusen und um Profile", Habilitationsschrift, Universität Karlsruhe (TH), Germany.
14. Sislian, J. P., 1975, "Condensation of Water Vapor with or without a Carrier Gas in a Shock Tube", UTIAS Report No.201.
15. Barschdorff, D., 1975, "Carrier Gas Effects on Homogeneous Nucleation of Water Vapor in a Shock Tube", The Physics of Fluids, 18:529-536.
16. Matsuo, K., Ikui, T., Setoguchi, T. and Kawagoe, S., 1981, "Relation between Condensation and Thermal Choking in an Unsteady Subsonic Flow", Bulletin of the JSME, 25:744-751.
17. Matsuo, S., Tanaka, M., Setoguchi, T. and Kim, H.D., 2002, "Shock Tube Flows with Non-equilibrium Condensation in Rarefaction Wave", *Proc. of the 13th International Symposium on Transport Phenomena (ISTP-13)*, 157-162.
18. Matsuo, S., Tanaka, M., Setoguchi, T. and Kim, H. D., Numerical Visualization of Moist Flow Through the Ludwieg Tube, International Journal of Transport Phenomena, to be published.
19. Yee, H.C., 1989, "A class of high-resolution explicit and implicit shock capturing methods", NASA TM-89464.
20. Baldwin, B.S. and Lomax, H., 1978, "Thin layer approximation and algebraic model for separated turbulent flows", AIAA paper, 78:257.
21. Adam, S., 1999, "Numerische und Exprimentelle Untersuchung Instationärer Düsenströmungen mit

Energiezufuhr durch Homogene Kondensation", Dissertation, Fukaltät für Maschinenbau, Universität Karlsruhe(TH), Germany.

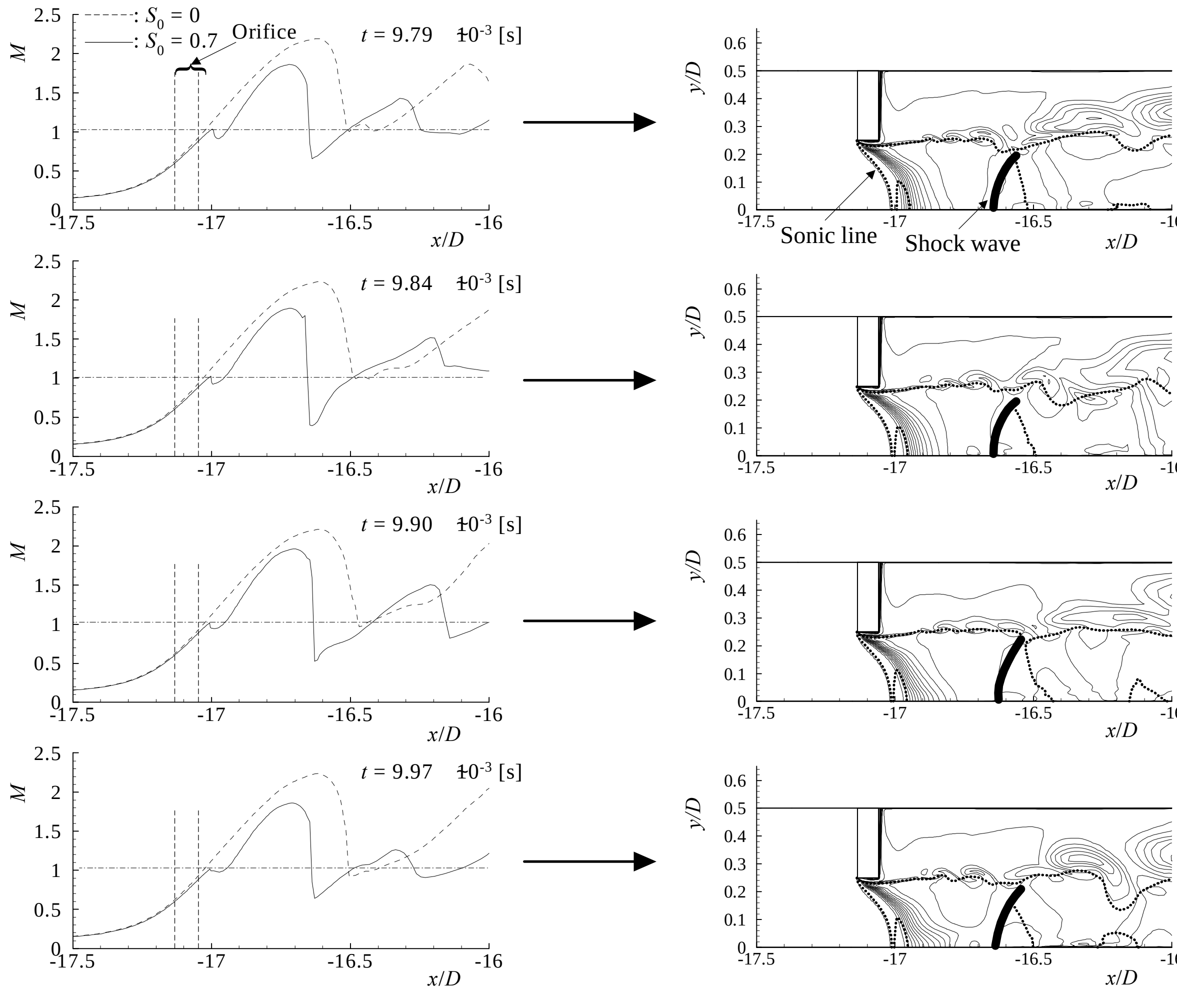

(a) Distribution of Mach number

(b) Contour maps of condensate mass fraction

Fig.7 Time variation of Mach number and condensate mass fraction (p_{41} = 5 , S_0 = 0.7)

6. NOMENCLATURE

Symbol	Meaning	Unit
C_p	Specific heat at constant pressure	(J/(kg · K))
E, ***F***	Numerical flux	(-)
E_s	Total energy per unit volume	(J/m^3)
g	Condensate mass fraction	(-)
H, ***Q***	Source term	(-)
I	Nucleation rate	(1/m^3 · s)
k	Boltzmann constant	(J/K)
L	Latent heat	(J/kg)
M	Molecular weight	(kg/kmol)
p	Static pressure	(Pa)
$p_{s,r}$	Saturation vapor pressure of condensate droplet with radius of *r*	(Pa)
$p_{s,\infty}$	Flat film equilibrium vapor pressure	(Pa)
R, ***S***	Viscous term	(-)
Re	Reynolds number	(-)
r	Droplet radius	(m)
r_c	Critical droplet radius	(m)
$\mathfrak{R}$	Gas constat	(J/(kg · K))
T	Temperature	(K)
t	Time	(s)
U	Conservation mass term	(-)
u, v	Cartesian velocity components	(m/s)
x, y	Cartesian coordinates	(m)
γ	Ratio of specific heats	(-)
ρ	Density	(kg/m^3)
σ	Surface tension	(N/m)
τ	Shear stress	(Pa)
	Subscripts	
0	Stagnation point	
1	Low pressure side	
2	Hot gas	
3	Cold gas	
4	High pressure side	
a	Air	
l	Liquid	
m	Mixture	
s	Saturattion	
v	Vapor	
∞	Plane surface	